



HAL
open science

Insights into the performance and mechanism of Cr(VI) and U(VI) removal in water using innovative cross-linked chitosan adsorbent

Peng Cheng, Zhiyang Wei, Yara Arbid, Tengfei Fu, Xiaowei Liu, Olivier Monfort

► To cite this version:

Peng Cheng, Zhiyang Wei, Yara Arbid, Tengfei Fu, Xiaowei Liu, et al.. Insights into the performance and mechanism of Cr(VI) and U(VI) removal in water using innovative cross-linked chitosan adsorbent. *Journal of Environmental Chemical Engineering*, 2024, 12 (1), pp.111731. 10.1016/j.jece.2023.111731 . hal-04467421

HAL Id: hal-04467421

<https://univ-rennes.hal.science/hal-04467421>

Submitted on 25 Apr 2024

HAL is a multi-disciplinary open access archive for the deposit and dissemination of scientific research documents, whether they are published or not. The documents may come from teaching and research institutions in France or abroad, or from public or private research centers.

L'archive ouverte pluridisciplinaire **HAL**, est destinée au dépôt et à la diffusion de documents scientifiques de niveau recherche, publiés ou non, émanant des établissements d'enseignement et de recherche français ou étrangers, des laboratoires publics ou privés.



Distributed under a Creative Commons Attribution - NonCommercial 4.0 International License

Insights into the performance and mechanism of Cr(VI) and U(VI) removal in water using innovative cross-linked chitosan adsorbent

Peng Cheng,^{abc} Zhiyang Wei,^d Yara Arbid,^e Tengfei Fu,^f Xiaowei Liu,^{a*} and Olivier Monfort^{g*}

- a. School of Biology Food and Environment, Hefei University, 230601 Hefei, China.
- b. Université Clermont Auvergne, CNRS, Clermont Auvergne INP, Institut de Chimie de Clermont Ferrand, F-63000 Clermont-Ferrand, France.
- c. Hubei Key Lab of Biomass Resource Chemistry and Environmental Biotechnology, School of Resources and Environmental Science, Wuhan University, Wuhan 430079, China.
- d. School of Resources and Environmental Engineering, Hefei University of Technology, 230009 Hefei, China.
- e. Univ. Rennes, École Nationale Supérieure de Chimie de Rennes, CNRS, ISCR-UMR 6226, F-35000 Rennes, France.
- f. Key Laboratory of Coastal Science and Integrated Management, First Institute of Oceanography, Ministry of Natural Resources of the People's Republic of China, Qingdao 266061, China.
- g. Department of Inorganic Chemistry, Faculty of Natural Sciences, Comenius University Bratislava, Ilkovicova 6, Mlynska Dolina, 84215 Bratislava, Slovakia.

*Corresponding authors: liuxw@hfut.edu.cn; monfort1@uniba.sk

Abstract

The primary aim of this work is to test a novel adsorbent prepared by cross-linking of tetrafluoroterephthalonitrile with chitosan (CS-TFT) for the removal of Cr(VI) and U(VI). The CS-TFT is stable until 250 °C and possesses amino functional groups due to the presence of CS that remain intact even after the cross-linking reaction, thus being a benefit for adsorption properties; while the TFT brought roughness to CS-TFT that keeps its high porosity. The adsorption efficiency of CS-TFT is evaluated in the batch experiment of Cr(VI) and U(VI) adsorption along with the effect of different experimental parameters (pH, time, temperature, initial concentrations, and co-existing inorganic cations). The maximum adsorption capacity of CS-TFT for adsorption of Cr(VI) and U(VI) was 265.96 mg·g⁻¹ at pH = 3 and 346.06 mg·g⁻¹ at pH = 5, respectively, at 298 K and the corresponding partition coefficients were 12454 and 6181 mg g⁻¹ mM⁻¹, respectively. The kinetics of the adsorption process is identified as a pseudo-second-order model and the Langmuir isotherm model is considered. The CS-TFT shows satisfactory reusability since it can be used after 6 cycles of regeneration with a removal efficiency of Cr(VI) and U(VI) higher than 90%. The adsorption mechanism is also proposed based on investigation of CS-TFT by FTIR, XPS and SEM-EDS before and after adsorption. The results show that hydroxy (OH) and amino (NH₂) groups play a key role in the chemical adsorption. All these findings suggest that CS-TFT could be a promising adsorbent for wastewaters treatment.

Keywords: Tetrafluoroterephthalonitrile; Cross-linked Chitosan; Chromium (VI); Uranium (VI); Adsorption; Partition coefficient

1. Introduction

The environmental pollution can affect all the compartments including air, water, and soil. Heavy metals and radionuclides are two kinds of highly toxic inorganic contaminants that can be found in soil and water, thus being a serious threat to the ecosystem and human health [1–3]. The heavy metals mainly include copper (Cu^{2+}), cadmium (Cd^{2+}), arsenic (As^{3+}), lead (Pb^{2+}), cobalt (Co^{2+}), chromium (Cr^{6+}), and mercury (Hg) [4] while radioactive pollutants include radium (^{226}Ra), uranium (^{235}U), cobalt (^{60}Co), polonium (^{210}Po), iodine (^{131}I), strontium (^{90}Sr), and cesium (^{137}Cs) [5]. In the present work, chromium (Cr(VI)) and uranium (U(VI)) are tested as model inorganic pollutants elements because of their strong carcinogenicity and high mobility [6]. For example, they can induce cell and DNA damage, causing organ failure [7,8]. The industrial sector, especially mining, is the main contributor to this contamination by the discharge of improperly cleaned wastewater [9]. Indeed, conventional treatment methods are not 100% efficient and they include coagulation-precipitation, membrane separation technology, ion exchange, and adsorption [4]. For example, the coagulation-precipitation method is very easily controlled and highly efficient, but it can produce a high amount of sludge and strongly affect the pH of waters. In addition, the membrane separation method has very high selectivity but with a very high cost. On the other hand, the adsorption method is one of the most widely used methods because of its simple operation and low cost. Innovative and efficient adsorbents are required to improve the removal efficiency of heavy metals and radionuclide contaminations [10–13].

Various materials have been developed as adsorbents for treating Cr(VI) and U(VI) , for instance, algae [14], layered double hydroxide (LDH) [15,16], and activated carbon [1]. Cr(VI) and U(VI) can transfer from the liquid phase to the solid surface by binding to the adsorbent through physical and/or chemical interactions. Chitosan (CS), which is known as a natural biopolymer, can be used as an adsorbent to remove a wide range of contaminants, such as heavy metals, radionuclides, and organic dyes [17,18]. In addition, CS is cheap, available, biodegradable, and non-toxic [17,18]. The preparation of CS is usually performed by the deacetylation of chitin [18], which is the most widespread biopolymer in nature (arthropods in marine environments produce more than 10^{12} kg of chitin per year) [19]. More importantly, the wastes from these arthropods can be reused, thus integrating the circular economy to produce CS. However, chitosan exhibits some disadvantages like low surface area, poor mechanical properties, and high solubility in acidic solution

[18,20]. Therefore, modification of CS by either physical or chemical methods is necessary to overcome these shortcomings [17,18].

One of the most frequently used techniques to improve such adsorbents is the cross-linking process since it increases the molecular weight. Therefore, such a method can improve the mechanical strength and chemical stability of CS, especially in an acidic solution [20]. Glyoxal, formaldehyde, glutaraldehyde, and epichlorohydrin are the most common cross-linking agents [17,18,20]. However, the cross-linking process can negatively affect the adsorption capacity of CS since it decreases the number of surface functional groups, like $-\text{OH}$ or $-\text{NH}_2$, that are involved in the adsorption process [20]. Hence, it is quite challenging to choose the appropriate cross-linking agent for achieving high mechanical strength, chemical stability, and an adequate number of surface functional groups.

A viable alternative is the use of tetrafluoroterephthalonitrile (TFT) as a cross-linking agent [21]. Indeed, Alsbaiee et al. have studied the TFT cross-linked β -cyclodextrin as an adsorbent to remove organic micropollutants in water [22]. Such an adsorbent has shown higher specific surface area after cross-linking reaction where the surface functional groups were still present, so the adsorption process could be efficient [22]. The explanation was that covalent bonds were formed between TFT and surface OH groups of β -cyclodextrin, thus remaining intact the other type of surface functional group that was involved in the adsorption process *i.e.*, $-\text{NH}_2$ [22].

In the present work, the tetrafluoroterephthalonitrile cross-linked chitosan (CS-TFT) adsorbent is prepared and used for the first time for the removal of Cr(VI) and U(VI), respectively. Along with the comprehensive characterization of CS-TFT, its performance is investigated at different experimental conditions and a mechanism of adsorption is proposed. In addition, since the surface CN group in TFT can be hydrolyzed into amide ($-\text{OCNH}_2$), it can potentially increase the number of active sites for adsorption [23]. This approach was also clarified for the first time here.

2. Materials and methods

2.1. Materials

Chitosan (CS, deacetylation degree $\geq 95\%$) and tetrafluoroterephthalonitrile (TFT, $C_8F_4N_2 \geq 99\%$) were purchased from Aladdin Reagent Co., Ltd. Tetrahydrofuran (THF, C_4H_8O , AR), potassium carbonate (K_2CO_3 , AR), and diphenylcarbazine ($C_{13}H_{14}N_4O$, AR) were purchased by Sinopharm Chemical Reagent Co., Ltd. Potassium dichromate ($K_2Cr_2O_7$, GR) was purchased from Tianjin Chemical Reagent Research Institute Co., Ltd. Uranium nitrate oxide ($UO_2(NO_3)_2$, GR) was purchased from Shanghai Macklin Biochemical Co., Ltd. Water (Milli-Q, resistivity $18\text{ M}\Omega\text{ cm}$, $DOC < 0.1\text{ mg L}^{-1}$) was used to prepare the solutions. All the chemicals were used without further purification.

2.2. Preparation of CS-TFT

The TFT cross-linked chitosan was prepared by nucleophilic substitution reaction. To this end, 1.5 g of CS and 100 mL of THF were mixed and sonicated for 15 min. Subsequently, 0.1 g of TFT and 1.5 g K_2CO_3 (catalyst) were added, and the mixture was ultrasonically shaken in an ice-water bath for 10 min, and the mixed solution was then stirred at $85\text{ }^\circ\text{C}$ in a water bath under nitrogen for 2 days and the refluxed solvent was collected using a condensing unit. After the filtration at ambient temperature, the obtained solid was washed with deionized water, methanol, and dichloromethane in sequence. Finally, after a drying process in a vacuum, the yellow CS-TFT powder was obtained. The reaction diagram is shown in **Figure S1**. A series of CS-TFT was prepared by using different concentrations of TFT solution *i.e.*, 2.5, 5.0, 7.5, 10.0, and 20.0 mM.

2.3 Characterization methods

The CS-TFT adsorbents were characterized using different methods. The FTIR analyses were recorded on an FTIR spectrometer (Thermo-Fischer Nicolet 380) equipped with advanced diamond ATR accessories (Specac-Golden Gate) to investigate the functional groups at the surface of CS-TFT. The morphology and microstructure of the adsorbent were recorded by an SEM (JSM-6490LV, JEOL) equipped with an energy-dispersive spectral analyzer (EDS). The BET analyses were carried out in a BET analyzer (Nova 3000e, Quantachrome). Zeta potential was determined by a laser particle size analyzer (ZEN 3700 Zetasizer, Malvern). The XPS measurements were conducted with an XPS spectrometer (Escalab 250Xi, Thermo Fisher) using $150\text{ W Al-K}\alpha$ X-ray radiations source to investigate the changes in chemical composition at the

surface resulting from (i) modification of CS by the TFT cross-linker and (ii) the adsorption of Cr(VI) and U(VI). The XPS data were processed using the CasaXPS program. Thermogravimetric (TG) and differential thermogravimetric (DTG) curves were recorded with a thermogravimetric analyzer (Netzsch TG209F1). All analyses were performed with 10 mg sample in air atmosphere. The temperature was set between 30 and 800 °C at a scanning rate of 10 °C min⁻¹.

2.4 Adsorption of Cr(VI) and U(VI)

The adsorption of Cr(VI) and U(VI) on CS-TFT was performed in batch experiments. In each experiment, 50 mg of CS-TFT was added into 100 mL 100 mg L⁻¹ Cr(VI) and U(VI) solutions, respectively. The suspension was put in a water bath at constant temperature and a speed of 200 rpm min⁻¹ for 3h. Then, aliquots of the mixture were sampled out at fixed interval times, filtrated with PTFE filters (CHROMAFIL® Xtra RC-20/25, 25 mm, Macherey-Nagel), and analyzed by UV-Visible spectrophotometer (AquaMate 8100, Thermo Fisher) to calculate the concentrations of Cr(VI) [24] and U(VI) [25], respectively. The effect of different experimental parameters on the adsorption capacity of CS-TFT was assessed and it included the TFT concentration (0-20 mM), pH (2-10), ion strength (0.01-1.00 M), and coexisting ions (K⁺, Na⁺, Ca²⁺, Mg²⁺, Al³⁺, Cu²⁺). The adsorption kinetics, adsorption isotherm, adsorption thermodynamics, and adsorbent reusability were also investigated. The adsorption kinetics data were fitted by using pseudo-first-order, pseudo-second-order, Elovich, and intraparticle-diffusion models. In addition, the adsorption isotherm data were studied by using Freundlich, Langmuir, Temkin, and D-R models. All adsorption experiments were run in triplicate, with a variation systematically less than 5%.

3. Results and discussion

3.1. Preparation and characterization of CS-TFT

3.1.1. Optimal amount of TFT

The amount of TFT is an important parameter since it can affect the adsorption properties of the final adsorbent. Indeed, a low amount of cross-linker does not form a stable cross-linked chitosan structure while a high amount leads to a decrease in active adsorption sites and specific surface area. The effect of the amount

of TFT on the adsorption properties of CS-TFT was investigated by preliminary tests *i.e.*, the removal efficiency of Cr(VI) and U(VI) at pH = 5 (**Figure 1**). The adsorption capacity of Cr(VI) and U(VI) increased with increasing the amount of TFT from 0.0 to 5.0 mM and then decreased with TFT increasing from 5.0 to 20.0 mM. Therefore, the optimal amount of TFT that is required during the preparation of CS-TFT is 5 mM, and all the following discussion is based on 5 mM TFT cross-linked chitosan.

3.1.2. Characterization of CS-TFT

The functional groups at the surface of CS and CS-TFT were analyzed by FTIR (**Figure 2a**). The characteristic absorption bands of chitosan (CS) were present. Indeed, the wide absorption band ranging from 3000 to 3700 cm^{-1} was assigned to the overlapping of the O–H and N–H stretching vibrations [26–28]. The bands at 2920 and 2876 cm^{-1} were ascribed to symmetric and asymmetric stretching of aliphatic C–H [26–28]. In addition, the bands at 1423 cm^{-1} were assigned to the $-\text{CH}_2$ bending [28]. It is interesting to notice the band at 1157 cm^{-1} which was attributed to the asymmetric stretching of bridge oxygen (*i.e.* glycosidic bond) [26,29], as well as the characteristic band for the C–H deformation of the β -glycosidic bond (at 894 cm^{-1}) [28]. Furthermore, the bands at around 1629 and 1325 cm^{-1} were assigned to the stretching vibration of the C=O bond [26,28] and the C–N bond [27,28], respectively. The band at 1382 cm^{-1} was assigned to secondary amide III [30]. Therefore, small amounts of amide groups were still present in commercial chitosan polymer chains. The bands at 1033 and 1087 cm^{-1} corresponded to C–O stretching vibration and bending frequencies of the C–OH groups of carbohydrates, respectively [30]. The band at 662 cm^{-1} was assigned to the N–H rocking vibration [26]. On the other hand, some discrepancies in the FTIR spectrum of TFT cross-linked chitosan (CS-TFT) were observed. Indeed, nitrile (C \equiv N) stretching vibration of TFT at 2235 cm^{-1} was not observed after cross-linking reaction [31]. Instead, the bending vibration of the N–H bond at 1606 cm^{-1} was detected [28], thus indicating that the nitrile (C \equiv N) group on the benzene ring of TFT had been converted to primary amide (O=C–NH₂) [23], thus being potentially used in the adsorption process.

To confirm the reaction between CS and TFT occurred and to further assess the differences in the surface chemical composition between CS and CS-TFT, the XPS characterization was performed (**Figure 2b**). The binding energy (BE) of the observed C1s, O1s, and N1s peaks along with their assignment were summarized in **Table S1**. The full XPS spectra of CS and CS-TFT (**Figure 2b1**) confirmed the presence of

carbon (C), oxygen (O), and nitrogen (N) in both CS and CS-TFT. However, fluorine (F) was only detected in CS-TFT, thus suggesting the cross-linked reaction between TFT and CS was successful (**Figure 2b1**). High-resolution C1s spectra for CS and CS-TFT represented an asymmetric peak that can be deconvoluted into several peaks, as shown in **Figures 2b2** and **2b3**, respectively. For CS, three deconvoluted peaks at 284.6 eV, 286.0 eV, and 287.6 eV corresponded to C–(C, H), C–(O, N), and O–C–O/O=C–N, respectively [32]. For CS-TFT, two additional deconvoluted peaks (**Figure 2b3**) at 292.6 eV and 295.6 eV corresponded to covalent and semi-ionic C–F bonds, respectively [33,34], thus indicating that TFT had been successfully cross-linked into CS. The high-resolution N1s spectra of both CS and CS-TFT (**Figure 2b4**) exhibited a symmetric peak at about 399.0 and 399.1 eV, which can be easily assigned to C–NH₂. Although the O1s peak which corresponds to C–(O, OH) was symmetric in CS (**Figure 2b5 - left**), this peak appeared asymmetric in CS-TFT (**Figure 2b5 - right**) and was deconvoluted into two peaks at 531.1 and 532.5 eV which were assigned to O=C=NH₂ and C–(O, OH), respectively. Finally, in **Figure 2b6**, the F1s peak which was only present in CS-TFT was an asymmetric peak that was deconvoluted into two peaks at 687.2 and 689.1 eV, thus corresponding to the covalent and semi-ionic C–F bond [33,34].

The morphology of CS and CS-TFT was investigated by SEM (**Figure 2c**). It was clearly observed that the particle size in CS-TFT (from 120-170 μm , **Figure 2c1**) was bigger than those in CS (70-100 μm , **Figure 2c3**) indicating that the cross-linking reaction was successful. Moreover, in CS, the particle surface was smooth and flat (**Figure 2c2**), while the surface of CS-TFT particles became rough after the cross-linking reaction (**Figure 2c4**). The increase in roughness was due to the surface modification caused by the cross-linking reaction. From the BET analysis (**Table S2**), the specific surface area of chitosan after cross-linking slightly increased from 2.6 to 2.9 $\text{m}^2 \text{g}^{-1}$, but the pore volume of CS-TFT (0.032 $\text{cm}^3 \text{g}^{-1}$) increased significantly compared to pure CS (0.004 $\text{cm}^3 \text{g}^{-1}$). Consequently, the TFT cross-linker led to an increase in the particle size of CS without negatively affecting the specific surface area, thus being a potential advantage for adsorption capacity. In addition, the surface of CS-TFT had been significantly modified in terms of chemical composition and morphology which are also potential advantages for adsorption processes. The stability of CS and CS-TFT was investigated by thermogravimetric analysis (TG/DTG) and results are shown in **Figure S2**. The CS and CS-TFT underwent two main stages of mass loss. The first stage of degradation occurred in the temperature range of 50~100°C, with a mass loss of 4% in CS-TFT (7% in CS), due to the

evaporation of adsorbed water [35]. The second stage occurred in the temperature range of 250 to 600 °C, with a mass loss of 63% in CS-TFT (61% in CS), which was assigned to the thermal decomposition of chitosan and elimination of volatile products [35]. For this second mass loss, a shift in the DTG peak value from 300 °C for pure CS to 306 °C for CS-TFT was observed, thus suggesting that the cross-linking reaction increased the thermal stability of CS-TFT.

To summarize the mechanism of synthesis of CS-TFT, the hydroxyl groups of the CS monomers underwent a nucleophilic substitution reaction with TFT in the presence of K_2CO_3 catalyst, thus leading to the cross-linking into CS-TFT. During the reaction, TFT lost fluorine atoms to form covalent bond with the oxygens of the hydroxyl group on CS. In addition, the nitrile group ($C\equiv N$) on the TFT was converted into a primary amide group. The reaction scheme for the cross-linking process was proposed in **Figure S3**.

3.2. Adsorption properties of CS-TFT

The effect of various experimental parameters including pH and ionic strength on the adsorption performance of CS-TFT were investigated while the adsorption kinetics and isotherms were determined. Since Cr(VI) and U(VI) are highly hazardous and toxic, the reusability of the innovative adsorbent was not investigated. It is worth noting that Q_{max} is widely used to indicate the performance of adsorbents, but its value can be affected by variables such as the adsorbent dosage, contact time, etc. Therefore, the partition coefficient (PC) was also used in this study to correlate the tendency observed using Q_{max} values [36]. In general, the higher the PC, the greater the adsorption affinity of the adsorbent *i.e.*, the adsorption affinity increases with increasing the partition coefficient (PC) which is defined as:

$$PC \text{ (mg g}^{-1} \mu\text{M}^{-1}) = Q_e/C_e \quad (\text{eq. 1})$$

where Q_e is the equilibrium adsorption capacity and C_e is the final adsorbate concentration [36,37].

3.2.1. Effect of initial pH on Cr(VI) and U(VI) adsorption

The pH is an important factor for the adsorption mechanism because it can influence the Zeta potential of the adsorbent and the ionic form of the pollutant in the solution [38]. Hence a wide range of pH (from 2

to 10) was used to study the effect of different initial pH for the adsorption of 100 mg L⁻¹ Cr(VI) and 20 mg L⁻¹ U(VI) solutions onto 0.2 g L⁻¹ CS-TFT (**Figure 3a**). The adsorption temperature was 308 K and the adsorption time was 3 h. The ionic strength was also investigated by the addition of NaCl (0.01, 0.1, and 1.0 M, respectively) (**Figure 3a**).

The speciation of Cr(VI) and U(VI) was simulated by Visual MINTEQ software, providing better insights into the adsorption process of these species (**Figures 3c and 3d**). For Cr(VI) adsorption, an increase in adsorption capacity was observed with the increase of pH from 2 to 3, and then it was followed by a strong decrease until pH = 4 (**Figure 3a**). It is worth noting that increasing the ionic strength led to a decrease in the adsorption capacity. This is due to the competitive adsorption between Cl⁻ and Cr⁶⁺. In addition, the point of zero charges (pH_{pzc}) of CS-TFT is at 6.44 (**Figure 3b**). Therefore, at pH < 6.44, the amino groups on the surface of CS-TFT are protonated i.e., its surface is positively charged. Since the predominant Cr(VI) species are HCrO₄⁻ at pH < 6.5 (**Figure 3c**), there are attractive electrostatic forces between the CS-TFT and the Cr(VI), thus leading to an efficient adsorption process, especially at pH = 3 (200 mg g⁻¹). Although a large amount of -NH₂ was protonated at pH = 3, the CS-TFT was not dissolved and still showed a high adsorption capacity, thus indicating the mechanical properties of CS were successfully consolidated by the TFT cross-linking process. However, at pH = 2, the value of the Zeta potential of CS-TFT was lower than the value at pH = 3, which probably was due to the structure of CS-TFT being partially destroyed at such a low pH. In addition, at pH between 4 and 6.44, the adsorption of Cr(VI) slightly decreases which is due to a decrease in the protonated amino group. Furthermore, at pH > 6.44, the surface of CS-TFT was negatively charged, thus CrO₄²⁻ (which was the predominant species in the solution according to **Figure 3c**) could not be adsorbed due to the electrostatic repulsion.

On the other hand, for the adsorption of U(VI) onto CS-TFT, the adsorption capacity increased with the increase of pH from 2 to 5, and then it was followed by a decrease in pH from 7 to 10 (**Figure 3a**). The effect of the ionic strength on U(VI) adsorption is similar to that of Cr(VI) adsorption. At pH < pH_{pzc}, the predominant U(VI) species are UO₂²⁺ and UO₂OH⁺ (**Figure 3d**), thus leading to electrostatic repulsion. However, the adsorption of U(VI) species was due to their coordination or complexation of the surface NH₂ group [39]. Therefore, the mechanism was different than in the case of Cr(VI), and adsorption capacity remained higher at pH from 4 to 7. At pH > 8, the predominant U(VI) species were (UO₂)₃(OH)₇⁻ and

$\text{UO}_2(\text{OH})_3^-$ (**Figure 3d**), so the electrostatic repulsion between CS-TFT and these species led to poor adsorption capacity.

3.2.2. Adsorption kinetics

The study of adsorption kinetics allowed us to obtain the time to reach the adsorption equilibrium, which is a crucial parameter for the design of the potential adsorption process for wastewater treatment plants. In **Figures S4a and S4b**, the adsorption kinetics of 100 mg L^{-1} Cr(VI) and 20 mg L^{-1} U(VI) on 0.2 g L^{-1} CS-TFT at $\text{pH} = 3.0$ and $\text{pH} = 5.0$, respectively, are shown. The removal of Cr(VI) and U(VI) by CS-TFT occurred significantly fast in the first 30 min and 60 min, respectively, before reaching equilibrium after about 60 min for Cr(VI) and 180 min for U(VI). The pseudo-first-order (eq. 2), pseudo-second-order (eq. 3), Elovich (eq. 4), and intraparticle diffusion (eq. 5) kinetic models were used to simulate the adsorption process [40]:

$$\ln(Q_e - Q_t) = \ln Q_e - K_1 t \quad (\text{eq. 2})$$

$$t/Q_t = 1/(K_2 \times Q_e^2) + t/Q_e \quad (\text{eq. 3})$$

$$Q_t = (1/\alpha) \ln t + (1/\alpha) \ln(\alpha\beta) \quad (\text{eq. 4})$$

$$Q_t = K_{int} t^{1/2} + C \quad (\text{eq. 5})$$

where Q_t (mg g^{-1}) and Q_e (mg g^{-1}) represent the adsorption extent of Cr(VI) or U(VI) at time t and equilibrium time e ; and K_1 (h^{-1}) and K_2 ($\text{g mg}^{-1} \text{ min}^{-1}$) represent the reaction rate constants of the pseudo-first-order and pseudo-second-order model, respectively. α and β represent the initial adsorption rate and desorption constant of the Elovich model [41]. K_{int} corresponds to the diffusion rate constant and C is a constant of the intraparticle diffusion model.

The calculated kinetic parameters are shown in **Table S3**. The pseudo-second-order kinetic model was more suitable to explain the adsorption process, thus indicating that the adsorption process was likely controlled by a chemical reaction process rather than a physical parameter [42]. Although the intra-particle diffusion model could be assumed, the adsorption processes can be divided into three stages, including (1) Cr(VI) and U(VI) diffusion from solutions to the surface of the adsorbent, (2) slow diffusion into the pores

and (3) the final equilibrium status. However, none of these stages passed through the origin, thus indicating that intraparticle diffusion is not the only rate-controlling step [43]. In addition, the Elovich model can also simulate the adsorption process well, suggesting that the adsorption of Cr(VI) and U(VI) could be controlled by a chemical process on a heterogeneous surface [44].

3.2.3. Adsorption isotherms

The adsorption isotherms of Cr(VI) and U(VI) on CS/TFT were monitored at 298, 308, and 318 K (**Figure 4**). The removal capacity of Cr(VI) and U(VI) by 0.2 g L⁻¹ CS-TFT decreased with increasing reaction temperature. Therefore, the adsorption process was promoted at a lower temperature because the removal of Cr(VI) and U(VI) is an exothermic process. In addition, the experimental data were fitted by Freundlich, Langmuir, Temkin, and D-R isotherm models (**Figure 4**). It is worth noting that the Langmuir model (eq. 6) is used to describe monolayer adsorption processes on a surface [45], while the Freundlich model (eq. 7) is used to describe heterogeneous adsorption [40,46].

$$C_e/Q_e = 1/(Q_{max} \times K_L) + C_e/Q_{max} \quad (\text{eq. 6})$$

$$\ln Q_e = \ln K_F + 1/n \times \ln C_e \quad (\text{eq. 7})$$

where Q_e (mg g⁻¹) is the amount of Cr(VI) and U(VI) adsorbed on CS-TFT; C_e is the equilibrium concentration; Q_{max} (mg g⁻¹) is the saturated sorption capacity; K_L is the Langmuir sorption constant; K_F and n are the Freundlich constants. These parameters are reported in **Table S4**.

Other models were also used to describe the adsorption isotherm including Temkin and D-R models. The Temkin model describes the effects of indirect adsorbate/adsorbate interactions on the adsorption process [47]. The heat of adsorption would decrease linearly with the coverage of the species in the layer due to the interactions between adsorbates. The Temkin model equation is the following [47]:

$$Q_e = B_1 \times \ln(A_T \times C_e) \quad (\text{eq. 8})$$

where A_T and B_1 correspond to the equilibrium binding constant (L mg⁻¹) and the heat of adsorption. $B_1 = RT/b$ where $T = 273$ K and $R = 8.314$ J mol⁻¹ K⁻¹.

By plotting Q_e as a function of C_e (**Figure 4a' and 4b'**), the B_I and A_T parameters can be determined (**Table S4**) and the heat of adsorption (B_I) decreased with increasing the temperature, thus indicating this adsorption process is exothermic [47].

Concerning the D-R model, it does not assume homogeneous surface or constant adsorption potential [48] and its mathematical form is the following:

$$\ln Q_e = \ln Q_s - B \times \varepsilon^2 \quad (\text{eq. 9})$$

with $\varepsilon = R \times T \times \ln(1 + 1/C_e)$ and Q_s is the D–R constant.

By plotting $\ln Q_e$ as a function of ε^2 (**Figure 4a'' and 4b''**), the Q_s and B can be determined (**Table S4**). The constant B is related to the free energy of sorption per molecule (E) in the following mathematical equation [48]:

$$E = 1/(2B)^{1/2} \quad (\text{eq. 10})$$

The type of the adsorption process can be identified thanks to the magnitude of E . The free energy for Cr(VI) and U(VI) adsorption was in the range of 995–2253 kJ mol⁻¹ and 287–460 kJ mol⁻¹, respectively, which were higher than the energy range of adsorption reactions i.e., 816 kJ/mol [48]. Therefore, it can be deduced that the type of adsorption for Cr(VI) and U(VI) onto CS-TFT was a chemical adsorption.

According to the coefficient of determination (R^2), the adsorption process was better fitted by the Langmuir model than the Freundlich model, thus indicating a monolayer adsorption process. Therefore, based on this model, the maximum adsorption capacity was 265.96 and 346.02 mg g⁻¹ at 298 K for Cr(VI) at pH = 3.0 and pH = 5.0, respectively (**Table S4**). For comparison with other chitosan-based adsorbents from the literatures, which were also used for the removal of Cr(VI) and U(VI), the present CS-TFT showed very high adsorption capacity (**Table 1**). Therefore, CS-TFT could find promising application output for wastewater treatment, especially for the removal of Cr(VI) and U(VI).

Table 1. Literature review of Cr(VI) and U(VI) adsorption using different adsorbents.

Elements	Material	Optimal pH	Adsorption Equilibrium Time (h)	Best-Fitted Isotherm Model	Q_{\max} (mg g ⁻¹)	Ref.
Cr(VI)	CS-TFT	3.0	1.0	Langmuir	265.96	This study
	Tetraethylenepentamine crosslinked chitosan oligosaccharide hydrogel	3.0	1.5	Langmuir	148.1	[49]

	Malic acid cross-linked chitosan	2.0	0.3	Langmuir	427.0	[50]
	Nanoscale FeS/chitosan/biochar composite	2.0	> 1.5	Freundlich	103.9	[51]
	Chitosan/ β -cyclodextrin beads	4.0	-	Freundlich	555.6	[52]
	Polyaniline@magnetic chitosan nanomaterials	2.0	1.0	Langmuir	186.6	[53]
	CS-TFT	6.0	1.0	Langmuir	346.0	This study
	Indole-functionalized cross-linked chitosan	6.5	6.0	Langmuir	847.5	[54]
U(VI)	Phosphorylation modification of hydrothermally cross-linked chitosan	5.5	0.5	Langmuir	384.6	[55]
	Nanoscale zero-valent iron loaded chitosan	6-8.0	0.5	Langmuir	591.7	[56]
	Polyvinylpyrrolidone/chitosan blended nanofibers	5.5-8.0	3.0	Freundlich	192.0	[57]

3.2.4. Adsorption thermodynamics

To evaluate the effect of temperature on the adsorption process of Cr(VI) and U(VI) on CS-TFT, the thermodynamic parameters were also calculated using the following equations:

$$\Delta G^\circ = -R \times T \times \ln K^\circ \quad (\text{eq. 11})$$

$$\Delta G^\circ = \Delta H^\circ - T \times \Delta S^\circ \quad (\text{eq. 12})$$

$$\ln K^\circ = \Delta S^\circ / R - \Delta H^\circ / (R \times T) \quad (\text{eq. 13})$$

where ΔG° , ΔH° , and ΔS° represent the change of Gibbs free energy, enthalpy, and entropy, respectively; R and T correspond to the ideal gas constant and the temperature (in K); K° is the adsorption equilibrium constant. Since the Langmuir model was assumed, K° can be calculated using the following equation [58]:

$$K^\circ = 1000 \times K_L \times M_A \times C^\circ \quad (\text{eq. 14})$$

where M_A and C° represent the molecular weight of adsorbate (L mol^{-1}) and the normal concentration (1 mol L^{-1}), respectively.

The calculated thermodynamic parameters are reported in **Table 2**. The negative value of ΔH° confirmed that the adsorption of the Cr(VI) and U(VI) process is an exothermic process, so the increase in

temperature is not conducive to the adsorption process. The negative values of ΔG° indicated the spontaneity of the Cr(VI) and U(VI) adsorption on CS-TFT.

Table 1. Thermodynamic data of Cr(VI) and U(VI) adsorption on CS-TFT

Elements	T (K)	ΔG° (kJ mol ⁻¹)	ΔH° (kJ mol ⁻¹)	ΔS° (J mol ⁻¹ K ⁻¹)
Cr(VI)	298K	-43.99		
	308K	-45.05	-13.12	102.96
	318K	-46.05		
U(VI)	298K	-39.35		
	308K	-40.42	-11.51	93.57
	318K	-41.22		

3.2.5. Adsorption discussion using partition coefficient

The PC represents the ratio of the concentration of the analyte in and on the solid adsorbent phase to its concentration in the liquid phase at the adsorption equilibrium [36,37]. The detailed experimental data of the PC under different parameters is shown in **Table S5**. For adsorption of Cr(VI), the highest values of PC for every single parameter, *i.e.*, pH = 3.0, adsorption time = 180 min, Cr(VI) concentration = 20 mg L⁻¹, and temperature = 298 K are 172.75, 274.81, 12454.67, and 12297.37 mg g⁻¹ mM⁻¹, respectively. On the other hand, similar results were obtained for adsorption of U(VI). Indeed, the highest PC values for U(VI) adsorption are 6181.00, 1651.87, 4076.81, and 4072.98 mg g⁻¹ mM⁻¹ at pH = 5.0, adsorption time = 180 min, and U(VI) concentration = 20 mg L⁻¹, and temperature = 298 K, respectively. For comparison, the PC values obtained for other materials used for the removal of Cr(VI) and U(VI) are reported in **Table S6**. It is clear that the present CS-TFT showed higher Cr(VI) and U(VI) adsorption performance ($\times 1000$ times higher Cr(VI) adsorption than SDS-chitosan [37]). Finally, one of the most important points is the high performance of CS-TFT obtained at low concentrations of contaminants, *i.e.*, showing high PC values. Therefore, it highlights that CS-TFT can be used to treat wastewater with low or trace concentrations of Cr(VI) and U(VI).

3.2.6. The selectivity and reusability of the CS-TFT

It is important to investigate whether the adsorbent is also efficient in media containing other species as wastewaters contaminated by Cr(VI) and U(VI) usually contain other inorganic metal ions. Therefore, to study the selectivity of CS-TFT, adsorption experiments were performed in solution containing Na^+ , Ca^{2+} , Mg^{2+} , Al^{3+} , and Cu^{2+} at 50 mg L^{-1} at $\text{pH} = 3$ for Cr(VI) removal (**Figure 5a**) and at 20 mg L^{-1} at $\text{pH} = 6$ for U(VI) removal (**Figure 5b**). At such conditions, the removal efficiency of Cr(VI) and U(VI) reached to 64.8% at $\text{pH} = 3.0$ and 99.7% at $\text{pH} = 6.0$ respectively. In regard with the removal efficiency of the other metal cations, the selectivity of CS-TFT towards Cr(VI) and U(VI) adsorption was satisfactory.

To test the reusability of CS-TFT, desorption of Cr(VI) and U(VI) (*i.e.*, regeneration of CS-TFT) was first performed before re-adsorption of these inorganic metal cations. Two different regeneration methods were utilized: (i) NaOH or HCl solutions and (ii) alkaline and acidic Na_2EDTA solutions. The reuse of CS-TFT for Cr(VI) adsorption after regeneration in alkaline solutions showed a removal efficiency in the range 98.2-99.3% at first utilization (**Figure 5c**). After 6 cycles, the Cr (VI) removal efficiency decreased slightly but still remained high *i.e.*, more than 90% (**Figure 5c**). This decrease might be attributed to the desorption that cannot remove 100% of the adsorbed Cr(VI) on the CS-TFT surface [59]. In **Figure 5d**, the reusability of CS-TFT for U(VI) adsorption after regeneration in acidic solutions is presented. The removal efficiency of U(VI) remained almost constant after 6 cycles *i.e.*, about 75% (**Figure 5d**). Overall, neither the desorption methods (regeneration) nor the reusability for Cr(VI) and U(VI) adsorption has an important impact of the efficiency of CS-TFT which is considered a stable adsorbent.

3.3. Insights into the adsorption mechanism

To understand the mechanism of Cr(VI) and U(VI) adsorption on CS-TFT, SEM, EDS, FTIR, and XPS were performed before and after adsorption processes. **Figure 6** shows the SEM images of CS-TFT after adsorption of Cr(VI) (**Figure 6a and 6a'**) and U(VI) (**Figure 6b and 6b'**). It can be seen from the EDS mapping (**Figure S5**) that Cr(VI) and U(VI) were successfully adsorbed on the CS-TFT surface, whereas the morphology of CSC-TFT (**Figures 6 and S5**) did not change significantly after adsorption. In addition, Cr(VI) and U(VI) are uniformly dispersed on the surface of CS-TFT after adsorption.

The FTIR spectra of CS-TFT after adsorption of Cr (VI) and U(VI) showed differences with pure CS-TFT (**Figure 6c**). Indeed, CS-TFT before adsorption exhibited peaks at 1087 , 1382 , and 1606 cm^{-1} that were

assigned to C-O bending vibrations of the C-OH groups, bending vibration of amide III, and N-H bending vibration, respectively. The Cr(VI) and U(VI) loaded adsorbent exhibited a shift of these peaks toward lower wavenumber *i.e.*, 1063, 1376, and 1587 cm^{-1} , respectively. In addition, the peak at 3449 cm^{-1} which corresponds to OH and N-H stretching vibration shifted to a lower wavenumber of 3323 cm^{-1} . These FTIR results suggested that the amino, amide, and hydroxyl groups of CS-TFT were the adsorption sites of for Cr(VI) and U(VI) ions, thus being consistent with a previous report [60].

XPS was performed to investigate the surface changes of CS-TFT, especially the chemical composition after adsorption (**Figure 7**). The full XPS spectra of CS-TFT after adsorption of Cr(VI) and U(VI) exhibited the characteristic peaks of chromium and uranium (**Figure 7a**), thus indicating their successful adsorption, *i.e.* their immobilization on the CS-TFT surface. Indeed, the high-resolution Cr2p spectrum (**Figure 7b**) consisted of two asymmetric peaks assigned to Cr2p_{1/2} and Cr2p_{3/2}. These peaks can be deconvoluted into Cr(VI) and Cr(III) signals, respectively at 587.5 eV and 585.5 eV (for Cr2p_{1/2}) and 578.3 eV and 576.0 eV (for Cr2p_{3/2}) [61]. In addition, the high-resolution U4f spectrum (**Figure 7c**) exhibited also two asymmetric peaks assigned to U4f_{7/2} and U4f_{5/2} and each of them can be deconvoluted into U(VI) signals (at 391.4 eV and 380.5 eV) and (IV) signals (at 389.7 eV and 378.9 eV) [62,63]. Therefore, Cr(VI) and U(VI) were reduced during the adsorption process probably due to the involvement of the lone electron pair on $-\text{NH}_2$ [64,65]. Since Cr(III) is less toxic and more stable than Cr(VI), and U(IV) is more likely to form precipitates than U(VI), the reduction process is an advantage in case of potential leaching from the adsorbent. Regarding these XPS results, it can be proposed that chromium and uranium were probably chemisorbed on the CS-TFT surface since reduction reactions occurred.

To confirm this hypothesis, the high-resolution spectra of N1s (**Figures 7d and 7e**) and O1s (**Figures 7f and 7g**) were investigated. After the adsorption of either Cr(VI) or U(VI), the asymmetric N1s peaks can be deconvoluted into three peaks at about 398.9 eV, 399.6 eV, and 401.6 eV. These peaks were attributed to the single bond with hydrogen ($-\text{NH}_2$), interaction with Cr(VI)/U(VI), and interaction with Cr(III)/U(IV), respectively [66]. Therefore, it indicated that electron transfer occurred between $-\text{NH}_2$ and Cr(VI) and U(VI), so reduction reactions took place *i.e.*, chemisorption [67,68]. Similarly, the high-resolution spectra of O1s exhibited asymmetric peaks that can be deconvoluted into three signals. Besides the peak of CS-TFT at 532.7 eV, two other ones at 530.2 eV and 530.5 eV were due to Cr(VI) and U(VI) adsorption and were assigned

to chromium and uranium oxides [69,70]. To resume, a proposed insight into the adsorption mechanism is the chemisorption of chromium and uranium (**Figure 8**).

4. Conclusion

The tetrafluoroterephthalonitrile cross-linked chitosan (CS-TFT) was for the first time prepared and tested for the removal of Cr(VI) and U(VI) in water. During the CS-TFT preparation, new surface functional groups were formed, especially $-O=C=NH_2$. The CS-TFT exhibited excellent adsorption capacity of Cr(VI) and U(VI) *i.e.*, $265.96 \text{ mg}\cdot\text{g}^{-1}$ at $\text{pH} = 3$ and $346.02 \text{ mg}\cdot\text{g}^{-1}$ at $\text{pH} = 5.0$, respectively. During the adsorption process, Cr(VI) and U(VI) were reduced to Cr(III) and U(IV) respectively. The proposed mechanism for the removal of Cr(VI) and U(VI) is a chemisorption process where the ions are immobilized on the surface of CS-TFT *via* interactions with hydroxy, amino, and amide groups. To conclude, CS-TFT is an innovative and efficient adsorbent that can be potentially applied at a larger scale for the removal of heavy metals and radionuclides in wastewater.

CRedit – authorship statement

Peng Cheng: Investigation, data analysis, Writing – original draft; Zhiyang Wei: Investigation, data analysis; Yara Arbid: Writing – review & editing; Tengfei Fu: Visualization, Writing – review & editing, Funding acquisition; Xiaowei Liu: Conceptualization, Writing – review & editing, Funding acquisition, Supervision; Olivier Monfort: Conceptualization, Writing – review & editing, Funding acquisition, Supervision.

Conflicts of interest

There are no conflicts to declare.

Acknowledgements

This research was partially supported by the Scientific Research Fund for Talents of Hefei University in 2021 (21-22RC30), the National Natural Science Foundation of China (42276226 and U1806212), the Natural Science Research Project of Higher Education in Anhui Province (KJ2021A1005), the Slovak Research and Development Agency (Contract No. APVV-21-0039), the Seed Fund Program for Sino-Foreign Joint Scientific Research Platform of Wuhan University (No. WHUZZJJ202217), and the project I-Site CAP 20–25 through the LIA (Laboratory of Environmental Processes Remediation). Peng Cheng also thanks the Chinese Scholarship Council for its financial support. Authors wish also to acknowledge Dr. Hongyu Lu for the help in the experiment operations.

References

- [1] Y. Song, G. Wei, M. Kopeć, L. Rao, Z. Zhang, E. Gottlieb, Z. Wang, R. Yuan, G. Ye, J. Wang, T. Kowalewski, K. Matyjaszewski, Copolymer-Templated Synthesis of Nitrogen-Doped Mesoporous Carbons for Enhanced Adsorption of Hexavalent Chromium and Uranium, *ACS Appl. Nano Mater.* 1 (2018) 2536–2543. <https://doi.org/10.1021/acsanm.8b00103>.
- [2] M. Thakare, H. Sarma, S. Datar, A. Roy, P. Pawar, K. Gupta, S. Pandit, R. Prasad, Understanding the holistic approach to plant-microbe remediation technologies for removing heavy metals and radionuclides from soil, *Curr. Res. Biotechnol.* 3 (2021) 84–98. <https://doi.org/10.1016/j.crbiot.2021.02.004>.
- [3] S. Das, S. Das, M.M. Ghangrekar, Efficacious bioremediation of heavy metals and radionuclides from wastewater employing aquatic macro- and microphytes, *J. Basic Microbiol.* 62 (2022) 260–278. <https://doi.org/10.1002/jobm.202100372>.
- [4] K.H. Vardhan, P.S. Kumar, R.C. Panda, A review on heavy metal pollution, toxicity and remedial measures: Current trends and future perspectives, *J. Mol. Liq.* 290 (2019) 111197. <https://doi.org/10.1016/j.molliq.2019.111197>.
- [5] S. Rajkhowa, J. Sarma, A. Rani Das, Chapter 15 - Radiological contaminants in water: pollution, health risk, and treatment, in: A. Ahamad, S.I. Siddiqui, P. Singh (Eds.), *Contam. Water*, Academic Press, 2021: pp. 217–236. <https://doi.org/10.1016/B978-0-12-824058-8.00013-X>.

- [6] F. Liu, A. Wang, M. Xiang, Q. Hu, B. Hu, Effective adsorption and immobilization of Cr(VI) and U(VI) from aqueous solution by magnetic amine-functionalized SBA-15, *Sep. Purif. Technol.* 282 (2022) 120042. <https://doi.org/10.1016/j.seppur.2021.120042>.
- [7] M. Balali-Mood, K. Naseri, Z. Tahergorabi, M.R. Khazdair, M. Sadeghi, Toxic Mechanisms of Five Heavy Metals: Mercury, Lead, Chromium, Cadmium, and Arsenic, *Front. Pharmacol.* 12 (2021). <https://www.frontiersin.org/articles/10.3389/fphar.2021.643972> (accessed November 22, 2023).
- [8] B.S. Canter, C.N. Leung, J.C. Fritton, T. Bäck, D. Rajon, E.I. Azzam, R.W. Howell, Radium-223–Induced Bystander Effects Cause DNA Damage and Apoptosis in Disseminated Tumor Cells in Bone Marrow, *Mol. Cancer Res.* 19 (2021) 1739–1750. <https://doi.org/10.1158/1541-7786.MCR-21-0005>.
- [9] T. Subba Rao, S. Panigrahi, P. Velraj, Chapter 21 - Transport and disposal of radioactive wastes in nuclear industry, in: S. Das, H.R. Dash (Eds.), *Microb. Biodegrad. Bioremediation Second Ed.*, Elsevier, 2022: pp. 419–440. <https://doi.org/10.1016/B978-0-323-85455-9.00027-8>.
- [10] M. Hao, Y. Liu, W. Wu, S. Wang, X. Yang, Z. Chen, Z. Tang, Q. Huang, S. Wang, H. Yang, X. Wang, Advanced porous adsorbents for radionuclides elimination, *EnergyChem.* 5 (2023) 100101. <https://doi.org/10.1016/j.enchem.2023.100101>.
- [11] Y. Li, T. Huang, X. Liu, Z. Chen, H. Yang, X. Wang, Sorption-catalytic reduction/extraction of hexavalent Cr(VI) and U(VI) by porous frameworks materials, *Sep. Purif. Technol.* 314 (2023) 123615. <https://doi.org/10.1016/j.seppur.2023.123615>.
- [12] J. Ru, B. Geng, C. Tong, H. Wang, S. Wu, H. Liu, Nanocellulose-Based Adsorption Materials, *Prog. Chem.* 29 (2017) 1228. <https://doi.org/10.7536/PC170616>.
- [13] Y. Wu, Y. Xie, X. Liu, Y. Li, J. Wang, Z. Chen, H. Yang, B. Hu, C. Shen, Z. Tang, Q. Huang, X. Wang, Functional nanomaterials for selective uranium recovery from seawater: Material design, extraction properties and mechanisms, *Coord. Chem. Rev.* 483 (2023) 215097. <https://doi.org/10.1016/j.ccr.2023.215097>.
- [14] G. Bayramoglu, A. Akbulut, M.Y. Arica, Study of polyethyleneimine-and amidoxime-functionalized hybrid biomass of *Spirulina (Arthrospira) platensis* for adsorption of uranium (VI) ion, *Environ. Sci. Pollut. Res.* 22 (2015) 17998–18010.

- [15] C. Muhire, D. Zhang, X. Xu, Adsorption of uranium (VI) ions by LDH intercalated with l-methionine in acidic water: Kinetics, thermodynamics and mechanisms, *Results Eng.* 16 (2022) 100686. <https://doi.org/10.1016/j.rineng.2022.100686>.
- [16] H.N. Tran, D.T. Nguyen, G.T. Le, F. Tomul, E.C. Lima, S.H. Woo, A.K. Sarmah, H.Q. Nguyen, P.T. Nguyen, D.D. Nguyen, T.V. Nguyen, S. Vigneswaran, D.-V.N. Vo, H.-P. Chao, Adsorption mechanism of hexavalent chromium onto layered double hydroxides-based adsorbents: A systematic in-depth review, *J. Hazard. Mater.* 373 (2019) 258–270. <https://doi.org/10.1016/j.jhazmat.2019.03.018>.
- [17] Y. Zhang, M. Zhao, Q. Cheng, C. Wang, H. Li, X. Han, Z. Fan, G. Su, D. Pan, Z. Li, Research progress of adsorption and removal of heavy metals by chitosan and its derivatives: A review, *Chemosphere.* 279 (2021) 130927.
- [18] S. (Gabriel) Kou, L.M. Peters, M.R. Mucalo, Chitosan: A review of sources and preparation methods, *Int. J. Biol. Macromol.* 169 (2021) 85–94. <https://doi.org/10.1016/j.ijbiomac.2020.12.005>.
- [19] M. Yadav, P. Goswami, K. Paritosh, M. Kumar, N. Pareek, V. Vivekanand, Seafood waste: a source for preparation of commercially employable chitin/chitosan materials, *Bioresour. Bioprocess.* 6 (2019) 1–20.
- [20] M.I. Wahba, Enhancement of the mechanical properties of chitosan, *J. Biomater. Sci. Polym. Ed.* 31 (2020) 350–375. <https://doi.org/10.1080/09205063.2019.1692641>.
- [21] X. Ma, I. Pinnau, A novel intrinsically microporous ladder polymer and copolymers derived from 1,1',2,2'-tetrahydroxy-tetraphenylethylene for membrane-based gas separation, *Polym. Chem.* 7 (2016) 1244–1248. <https://doi.org/10.1039/C5PY01796C>.
- [22] A. Alsbaiee, B.J. Smith, L. Xiao, Y. Ling, D.E. Helbling, W.R. Dichtel, Rapid removal of organic micropollutants from water by a porous β -cyclodextrin polymer, *Nature.* 529 (2016) 190–194.
- [23] V. Theodorou, G. Paraskevopoulos, K. Skobridis, A mild alkaline hydrolysis of N- and N,N-substituted amides and nitriles, *Arkivoc.* 2015 (2015) 101–112. <https://doi.org/10.3998/ark.5550190.p009.205>.
- [24] J. Ščančar, T. Osterman, N. Bukovec, R. Mllacic, Critical appraisal of analytical procedures for the determination of CR(VI) in dyed leathers by 1,5 diphenylcarbazide spectrophotometry after sample dilution or color removal, *J. Am. Leather Chem. Assoc.* 102 (2007) 85–92.

- [25] R. Thakur, P.K. Tarafder, R.R. Jha, A novel method for the determination of uranium and free acidity in nuclear fuel process samples by extraction spectrophotometry, *Radiochim. Acta.* 107 (2019) 327–337. <https://doi.org/10.1515/ract-2018-2965>.
- [26] K. Ahmed Ismail, A. El Askary, M.O. Farea, N.S. Awwad, H.A. Ibrahim, M. Eid Moustapha, A.A. Menazea, Perspectives on composite films of chitosan-based natural products (Ginger, Curcumin, and Cinnamon) as biomaterials for wound dressing, *Arab. J. Chem.* 15 (2022) 103716. <https://doi.org/10.1016/j.arabjc.2022.103716>.
- [27] A. Saleem, N. Akhtar, M.U. Minhas, A. Mahmood, K.U. Khan, O. Abdullah, Highly Responsive Chitosan-Copoly (MAA) Nanomatrices through Cross-Linking Polymerization for Solubility Improvement, *Gels.* 8 (2022) 196. <https://doi.org/10.3390/gels8030196>.
- [28] S. Saha, T.K. Saha, S. Karmaker, Z. Islam, S. Demeshko, H. Frauendorf, F. Meyer, Solar Light-Assisted Oxidative Degradation of Ciprofloxacin in Aqueous Solution by Iron(III) Chelated Cross-Linked Chitosan Immobilized on a Glass Plate, *Catalysts.* 12 (2022) 475. <https://doi.org/10.3390/catal12050475>.
- [29] N.M. Ahyat, F. Mohamad, A. Ahmad, A.A. Azmi, Chitin and chitosan extraction from *Portunus pelagicus*, *Malays. J. Anal. Sci.* 21 (2017) 770–777.
- [30] J. Tantala, K. Thumanu, C. Rachtanapun, An assessment of antibacterial mode of action of chitosan on *Listeria innocua* cells using real-time HATR-FTIR spectroscopy, *Int. J. Biol. Macromol.* 135 (2019) 386–393. <https://doi.org/10.1016/j.ijbiomac.2019.05.032>.
- [31] X. Liang, R. Ma, L. Hao, C. Wang, Q. Wu, Z. Wang, β -Cyclodextrin polymer@Fe₃O₄ based magnetic solid-phase extraction coupled with HPLC for the determination of benzoylurea insecticides from honey, tomato, and environmental water samples, *J. Sep. Sci.* 41 (2018) 1539–1547. <https://doi.org/10.1002/jssc.201701197>.
- [32] A. Skwarczynska, M. Kaminska, P. Owczarz, N. Bartoszek, B. Walkowiak, Z. Modrzejewska, The structural (FTIR, XRD, and XPS) and biological studies of thermosensitive chitosan chloride gels with β -glycerophosphate disodium, *J. Appl. Polym. Sci.* 135 (2018) 46459.
- [33] Y. Zhao, K.X. Yao, B. Teng, T. Zhang, Y. Han, A perfluorinated covalent triazine-based framework for highly selective and water-tolerant CO₂ capture, *Energy Environ. Sci.* 6 (2013) 3684–3692. <https://doi.org/10.1039/C3EE42548G>.

- [34] Y. Wang, J. Chen, G. Wang, Y. Li, Z. Wen, Perfluorinated covalent triazine framework derived hybrids for the highly selective electroconversion of carbon dioxide into methane, *Angew. Chem. Int. Ed.* 57 (2018) 13120–13124.
- [35] V.-P. Dinh, M.-D. Nguyen, Q.H. Nguyen, T.-T.-T. Do, T.-T. Luu, A.T. Luu, T.D. Tap, T.-H. Ho, T.P. Phan, T.D. Nguyen, L.V. Tan, Chitosan-MnO₂ nanocomposite for effective removal of Cr (VI) from aqueous solution, *Chemosphere*. 257 (2020) 127147. <https://doi.org/10.1016/j.chemosphere.2020.127147>.
- [36] Y. Xiao, A.S. Helal, E. Mazario, A. Mayoral, A. Chevillot-Biraud, P. Decorse, R. Losno, F. Maurel, S. Ammar, J.S. Lomas, Functionalized maghemite nanoparticles for enhanced adsorption of uranium from simulated wastewater and magnetic harvesting, *Environ. Res.* (2022) 114569.
- [37] X. Du, C. Kishima, H. Zhang, N. Miyamoto, N. Kano, Removal of chromium (VI) by chitosan beads modified with sodium dodecyl sulfate (SDS), *Appl. Sci.* 10 (2020) 4745.
- [38] W. Liu, Q. Wang, H. Wang, Q. Xin, W. Hou, E. Hu, Z. Lei, Adsorption of uranium by chitosan/*Chlorella pyrenoidosa* composite adsorbent bearing phosphate ligand, *Chemosphere*. 287 (2022) 132193. <https://doi.org/10.1016/j.chemosphere.2021.132193>.
- [39] X. Tang, L. Zhou, Z. Le, Y. Wang, Z. Liu, G. Huang, A.A. Adesina, Preparation of porous chitosan/carboxylated carbon nanotube composite aerogels for the efficient removal of uranium(VI) from aqueous solution, *Int. J. Biol. Macromol.* 160 (2020) 1000–1008. <https://doi.org/10.1016/j.ijbiomac.2020.05.179>.
- [40] W.-J. Ma, T.-H. Chen, D. Chen, H.-B. Liu, P. Cheng, Z.-X. Zhang, Q. Tao, Y.-Z. Zhang, Removal of Fe (II), Mn (II), and NH₄⁺-N by Using δ-MnO₂ Coated Zeolite, *Huan Jing Ke Xue Huanjing Kexue*. 40 (2019) 4553–4561.
- [41] F.-C. Wu, R.-L. Tseng, R.-S. Juang, Characteristics of Elovich equation used for the analysis of adsorption kinetics in dye-chitosan systems, *Chem. Eng. J.* 150 (2009) 366–373. <https://doi.org/10.1016/j.cej.2009.01.014>.
- [42] P. Cheng, D. Chen, H. Liu, X. Zou, Y. Zhang, J. Xie, C. Qing, T. Chen, Enhanced adsorption capacity for phosphate in wastewater from thermally activated flue gas desulfurization gypsum, *J. Chem. Technol. Biotechnol.* 93 (2018) 1733–1741. <https://doi.org/10.1002/jctb.5546>.

- [43] B. Guo, Y. Wang, X. Qiao, X. Shen, J. Guo, J. Xiang, Y. Jin, Experiment and regeneration kinetic model study on CO₂ adsorbent prepared from fly ash, *Chem. Eng. J.* 421 (2021) 127865. <https://doi.org/10.1016/j.cej.2020.127865>.
- [44] C. Lin, W. Luo, T. Luo, Q. Zhou, H. Li, L. Jing, A study on adsorption of Cr (VI) by modified rice straw: Characteristics, performances and mechanism, *J. Clean. Prod.* 196 (2018) 626–634. <https://doi.org/10.1016/j.jclepro.2018.05.279>.
- [45] Y.-T. Zhou, H.-L. Nie, C. Branford-White, Z.-Y. He, L.-M. Zhu, Removal of Cu²⁺ from aqueous solution by chitosan-coated magnetic nanoparticles modified with α -ketoglutaric acid, *J. Colloid Interface Sci.* 330 (2009) 29–37. <https://doi.org/10.1016/j.jcis.2008.10.026>.
- [46] P. Cheng, D. Chen, H. Liu, X. Zou, Z. Wu, J. Xie, C. Qing, D. Kong, T. Chen, Synergetic effects of anhydrite and brucite-periclase materials on phosphate removal from aqueous solution, *J. Mol. Liq.* 254 (2018) 145–153.
- [47] R.A. Abu-Zurayk, R.Z. Al Bakain, I. Hamadneh, A.H. Al-Dujaili, Adsorption of Pb(II), Cr(III) and Cr(VI) from aqueous solution by surfactant-modified diatomaceous earth: Equilibrium, kinetic and thermodynamic modeling studies, *Int. J. Miner. Process.* 140 (2015) 79–87. <https://doi.org/10.1016/j.minpro.2015.05.004>.
- [48] Y. Fang, J. Wen, G. Zeng, F. Jia, S. Zhang, Z. Peng, H. Zhang, Effect of mineralizing agents on the adsorption performance of metal–organic framework MIL-100(Fe) towards chromium(VI), *Chem. Eng. J.* 337 (2018) 532–540. <https://doi.org/10.1016/j.cej.2017.12.136>.
- [49] J. Mei, H. Zhang, Z. Li, H. Ou, A novel tetraethylenepentamine crosslinked chitosan oligosaccharide hydrogel for total adsorption of Cr(VI), *Carbohydr. Polym.* 224 (2019) 115154. <https://doi.org/10.1016/j.carbpol.2019.115154>.
- [50] S. Sethi, S. Thakur, D. Sharma, G. Singh, N. Sharma, B.S. Kaith, S. Khullar, Malic acid cross-linked chitosan based hydrogel for highly effective removal of chromium (VI) ions from aqueous environment, *React. Funct. Polym.* 177 (2022) 105318. <https://doi.org/10.1016/j.reactfunctpolym.2022.105318>.
- [51] Y. Yang, Y. Zhang, G. Wang, Z. Yang, J. Xian, Y. Yang, T. Li, Y. Pu, Y. Jia, Y. Li, Z. Cheng, S. Zhang, X. Xu, Adsorption and reduction of Cr(VI) by a novel nanoscale FeS/chitosan/biochar composite from aqueous solution, *J. Environ. Chem. Eng.* 9 (2021) 105407. <https://doi.org/10.1016/j.jece.2021.105407>.

- [52] T. Kekes, G. Kolliopoulos, C. Tzia, Hexavalent chromium adsorption onto crosslinked chitosan and chitosan/ β -cyclodextrin beads: Novel materials for water decontamination, *J. Environ. Chem. Eng.* 9 (2021) 105581. <https://doi.org/10.1016/j.jece.2021.105581>.
- [53] C. Lei, C. Wang, W. Chen, M. He, B. Huang, Polyaniline@magnetic chitosan nanomaterials for highly efficient simultaneous adsorption and in-situ chemical reduction of hexavalent chromium: Removal efficacy and mechanisms, *Sci. Total Environ.* 733 (2020) 139316. <https://doi.org/10.1016/j.scitotenv.2020.139316>.
- [54] Y. Wang, Y. Ai, X. Liu, B. Chen, Y. Zhang, Indole-functionalized cross-linked chitosan for effective uptake of uranium (vi) from aqueous solution, *Polym. Chem.* 13 (2022) 1751–1762.
- [55] Y. Sun, Y. Kang, W. Zhong, Y. Liu, Y. Dai, A simple phosphorylation modification of hydrothermally cross-linked chitosan for selective and efficient removal of U(VI), *J. Solid State Chem.* 292 (2020) 121731. <https://doi.org/10.1016/j.jssc.2020.121731>.
- [56] Q. Zhang, D. Zhao, S. Feng, Y. Wang, J. Jin, A. Alsaedi, T. Hayat, C. Chen, Synthesis of nanoscale zero-valent iron loaded chitosan for synergistically enhanced removal of U(VI) based on adsorption and reduction, *J. Colloid Interface Sci.* 552 (2019) 735–743. <https://doi.org/10.1016/j.jcis.2019.05.109>.
- [57] Y. Liu, Y. Liu, X. Cao, R. Hua, Y. Wang, C. Pang, M. Hua, X. Li, Biosorption studies of uranium (VI) on cross-linked chitosan: isotherm, kinetic and thermodynamic aspects, *J. Radioanal. Nucl. Chem.* 290 (2011) 231–239. <https://doi.org/10.1007/s10967-011-1336-z>.
- [58] L.Y. Na, L.Y. Zhang, F.J. Zhang, R.N. Hua, Calculation of Adsorption Thermodynamic Parameters at Solid-liquid Interfaces, *Mater Rep.* 34 (2020) 22030–22035.
- [59] A. Herath, C.A. Layne, F. Perez, E.B. Hassan, C.U. Pittman, T.E. Mlsna, KOH-activated high surface area Douglas Fir biochar for adsorbing aqueous Cr(VI), Pb(II) and Cd(II), *Chemosphere.* 269 (2021) 128409. <https://doi.org/10.1016/j.chemosphere.2020.128409>.
- [60] L. Ren, J. Xu, Y. Zhang, J. Zhou, D. Chen, Z. Chang, Preparation and characterization of porous chitosan microspheres and adsorption performance for hexavalent chromium, *Int. J. Biol. Macromol.* 135 (2019) 898–906. <https://doi.org/10.1016/j.ijbiomac.2019.06.007>.
- [61] L. Zhang, W. Xia, X. Liu, W. Zhang, Synthesis of titanium cross-linked chitosan composite for efficient adsorption and detoxification of hexavalent chromium from water, *J. Mater. Chem. A.* 3 (2015) 331–340.

- [62] H. Wang, H. Guo, N. Zhang, Z. Chen, B. Hu, X. Wang, Enhanced Photoreduction of U(VI) on C₃N₄ by Cr(VI) and Bisphenol A: ESR, XPS, and EXAFS Investigation, *Environ. Sci. Technol.* 53 (2019) 6454–6461. <https://doi.org/10.1021/acs.est.8b06913>.
- [63] L. Zhang, Y. Li, H. Guo, H. Zhang, N. Zhang, T. Hayat, Y. Sun, Decontamination of U(VI) on graphene oxide/Al₂O₃ composites investigated by XRD, FT-IR and XPS techniques, *Environ. Pollut.* 248 (2019) 332–338. <https://doi.org/10.1016/j.envpol.2019.01.126>.
- [64] L. Liu, W. Cai, C. Dang, B. Han, Y. Chen, R. Yi, J. Fan, J. Zhou, J. Wei, One-step vapor-phase assisted hydrothermal synthesis of functionalized carbons: Effects of surface groups on their physicochemical properties and adsorption performance for Cr (VI), *Appl. Surf. Sci.* 528 (2020) 146984.
- [65] X. Zhong, Y. Liu, W. Zeng, Y. Zhu, B. Hu, Excellent photoreduction performance of U(VI) on metal organic framework/covalent organic framework heterojunction by solar-driven, *Sep. Purif. Technol.* 285 (2022) 120405. <https://doi.org/10.1016/j.seppur.2021.120405>.
- [66] M. Wang, Y. She, Z. Xiao, J. Hu, R. Zhou, J. Zhang, The green adsorption of chitosan tripolyphosphate nanoparticles on cotton fiber surfaces, *Carbohydr. Polym.* 101 (2014) 812–818.
- [67] Z. Chen, J. Wang, M. Hao, Y. Xie, X. Liu, H. Yang, G.I.N. Waterhouse, X. Wang, S. Ma, Tuning excited state electronic structure and charge transport in covalent organic frameworks for enhanced photocatalytic performance, *Nat. Commun.* 14 (2023) 1106. <https://doi.org/10.1038/s41467-023-36710-x>.
- [68] M. Hao, Y. Xie, X. Liu, Z. Chen, H. Yang, G.I.N. Waterhouse, S. Ma, X. Wang, Modulating Uranium Extraction Performance of Multivariate Covalent Organic Frameworks through Donor–Acceptor Linkers and Amidoxime Nanotraps, *JACS Au.* 3 (2023) 239–251. <https://doi.org/10.1021/jacsau.2c00614>.
- [69] R. Bhatt, B. Sreedhar, P. Padmaja, Adsorption of chromium from aqueous solutions using crosslinked chitosan–diethylenetriaminepentaacetic acid, *Int. J. Biol. Macromol.* 74 (2015) 458–466. <https://doi.org/10.1016/j.ijbiomac.2014.12.041>.
- [70] D. Pan, Q. Fan, F. Fan, Y. Tang, Y. Zhang, W. Wu, Removal of uranium contaminant from aqueous solution by chitosan@attapulgit composite, *Sep. Purif. Technol.* 177 (2017) 86–93. <https://doi.org/10.1016/j.seppur.2016.12.026>.

Figures

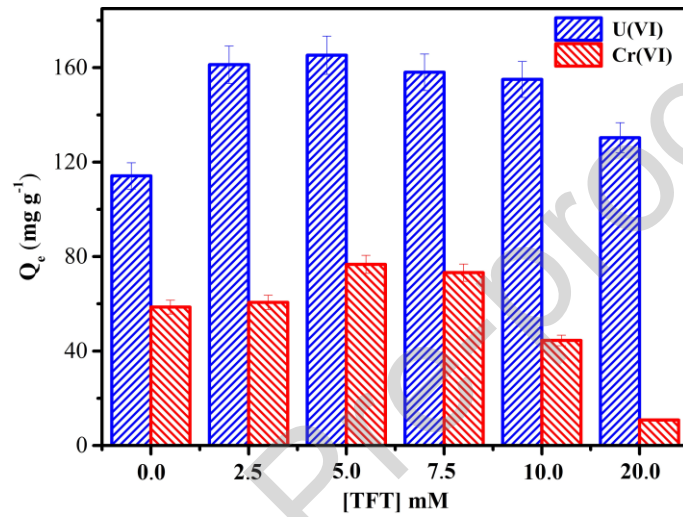


Figure 1. The effect of the amount of cross-link agent (TFT) on the adsorption capacity of Cr(VI) and U(VI) at CS-TFT. [CS-TFT] = 0.5 g L^{-1} ; [Cr(VI)] = [U(VI)] = 100 mg L^{-1} ; Adsorption time = 3 h; pH = 5.0

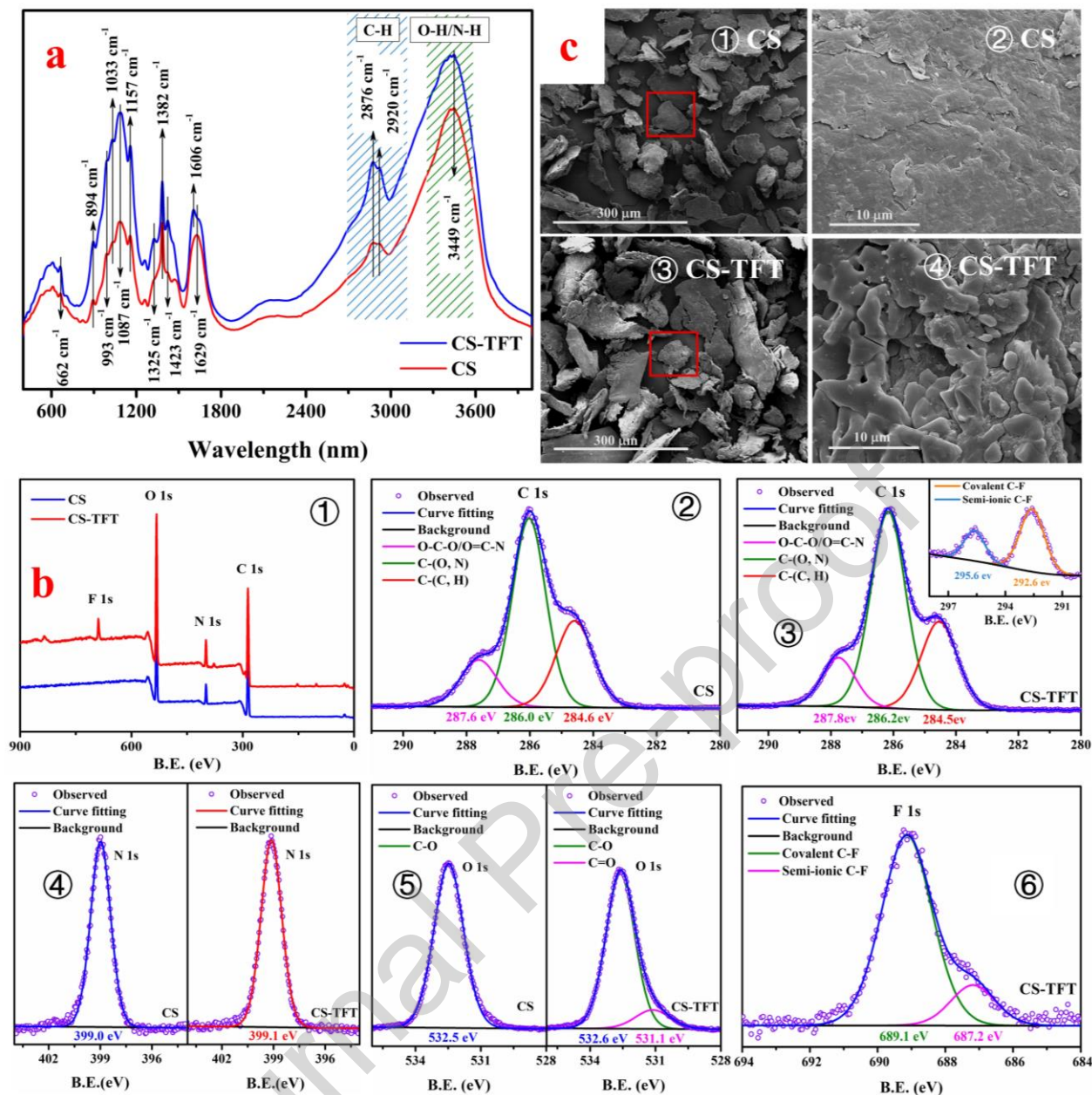


Figure 2. (a) The FTIR spectra of CS and CS-TFT; (b) The XPS spectra of CS and CS-TFT: (b1) full scan, and high-resolution spectrum of (b2, b3) C1s, (b4) N1s, (b5) O1s, and (b6) F1s; (c) Low and high magnification SEM images of CS (c1, c2) and CS-TFT (c3, c4) - the high magnification images were taken at the red framed area

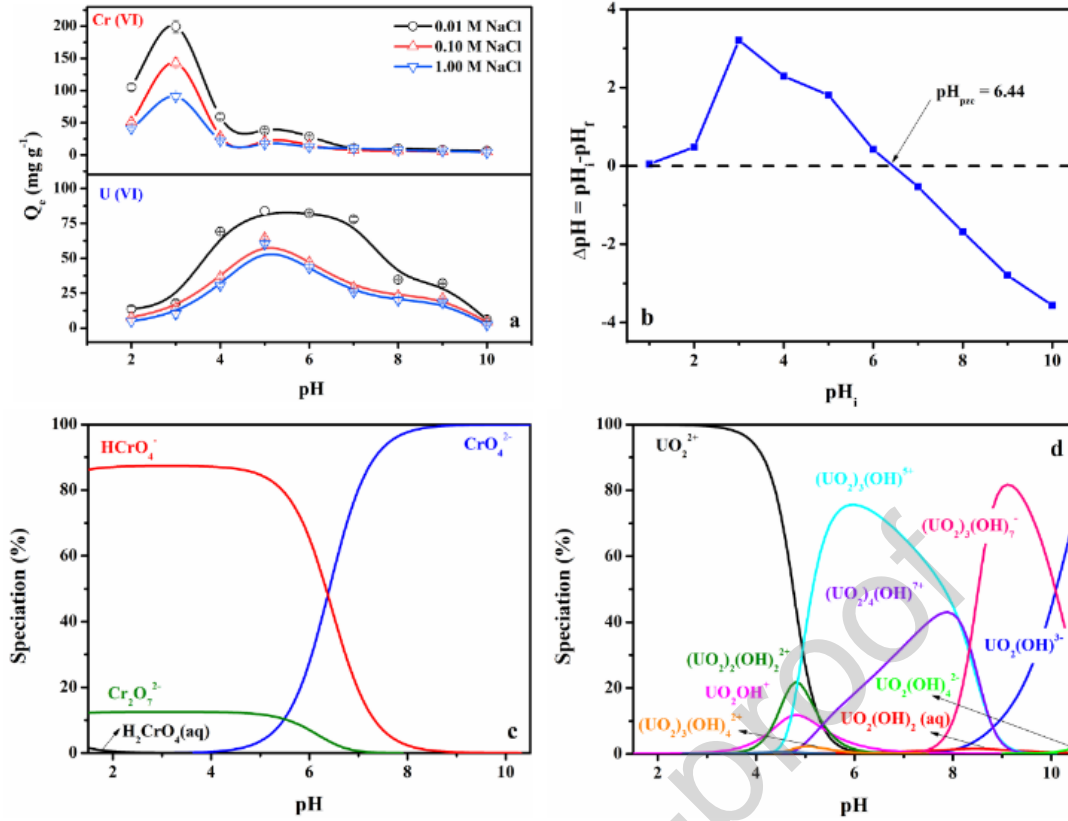


Figure 3. The effect of different pH and ionic strength on the adsorption of Cr(VI) and U(VI) onto CS-TFT (a). [CS-TFT] = 0.2 g L^{-1} , [Cr(VI)] = 100 mg L^{-1} or [U(VI)] = 20 mg L^{-1} ; T = 308K; The Zeta potential of CS-TFT (b). The speciation of 100 mg L^{-1} Cr(VI) and 20 mg L^{-1} U(VI) as a function of pH with 0.01 M ionic strength was obtained by the Visual MINTEQ program (c and d).

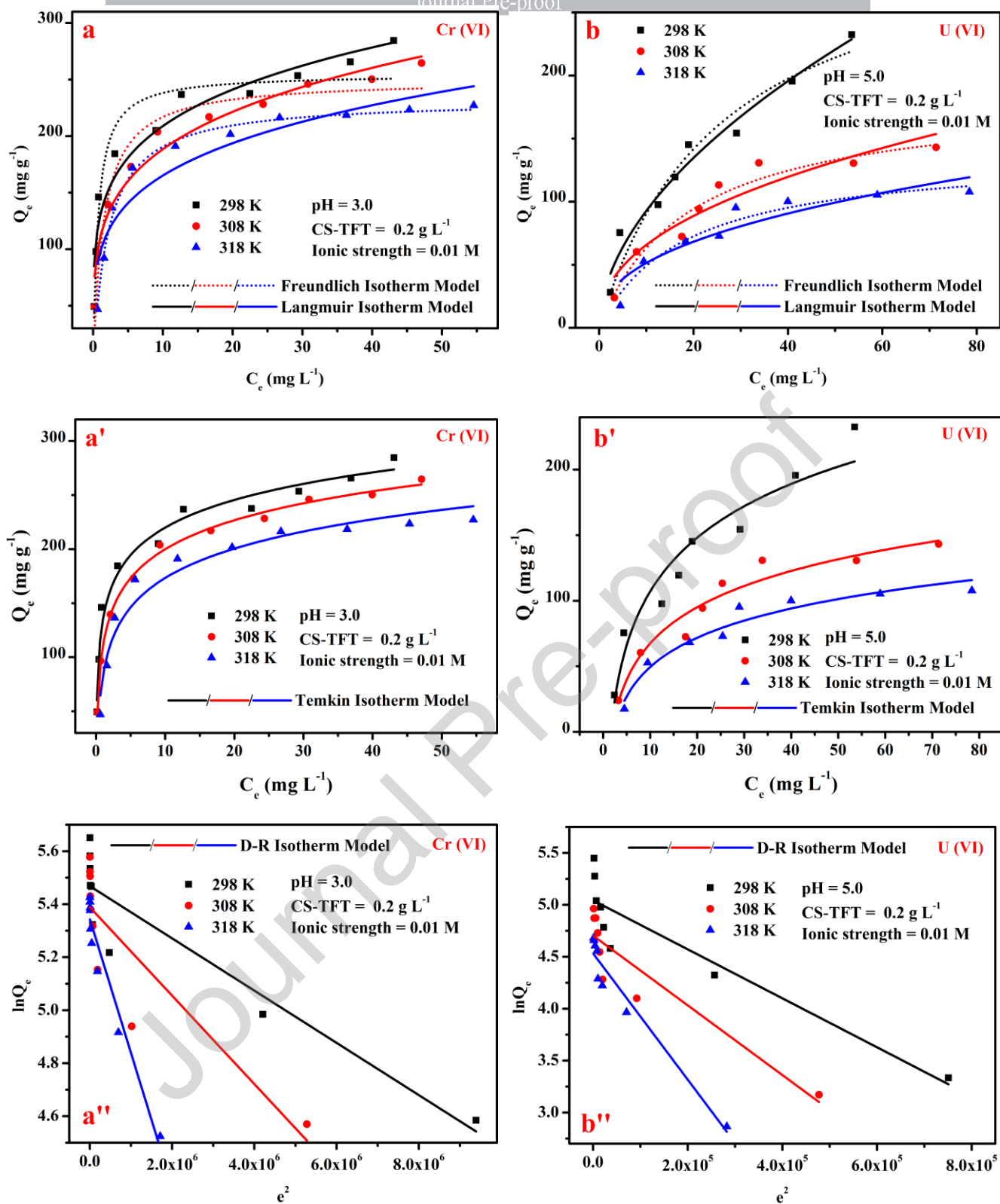


Figure 4. Adsorption isotherms at three different temperatures by using Freundlich, Langmuir, Temlin, and D-R models for adsorption of (a, a' and a'') Cr(VI) and (b, b' and b'') U(VI) on CS-TFT.

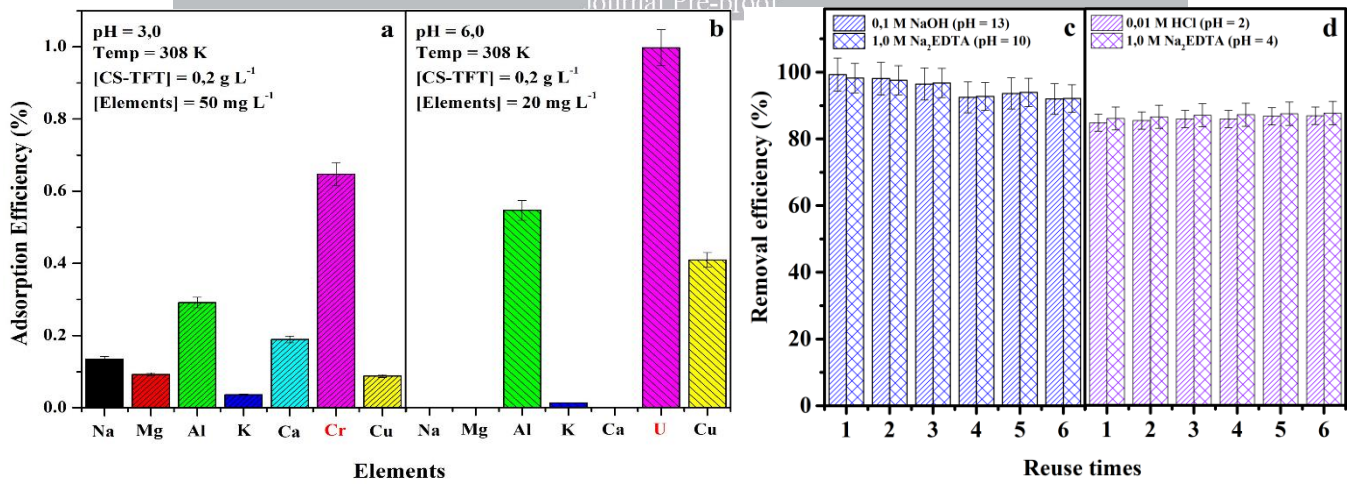


Figure 5. The selectivity (a, b) and the reusability of CS-TFT for adsorption of (c) Cr(VI) and (d) U(VI).

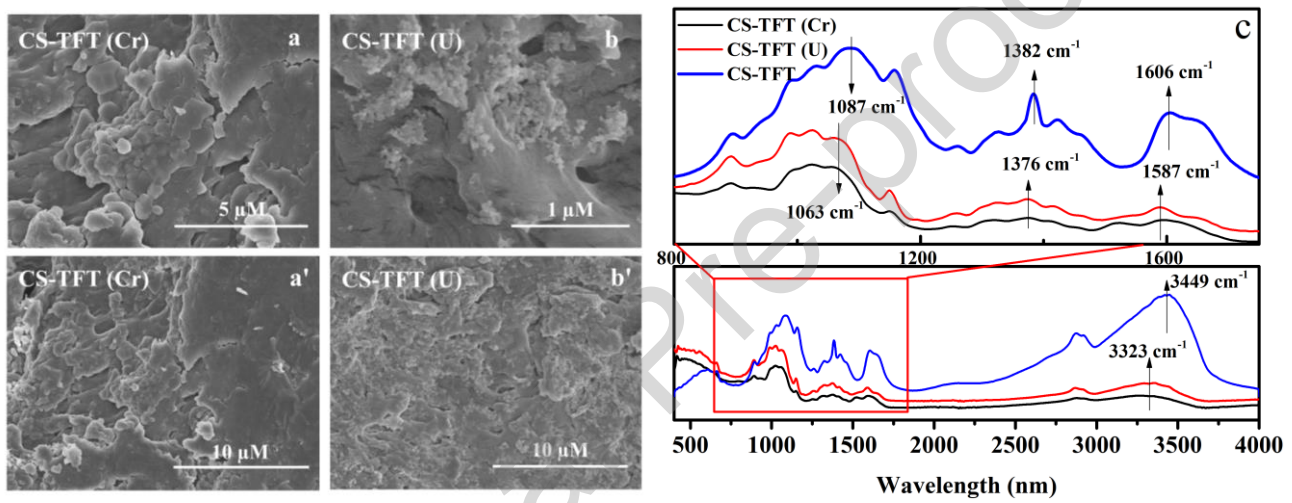


Figure 6. SEM images CS-TFT after adsorption of (a and a') Cr(VI) and (b and b') U(VI). (c) FTIR spectra of CS-TFT before and after adsorption of Cr(VI) and U(VI).

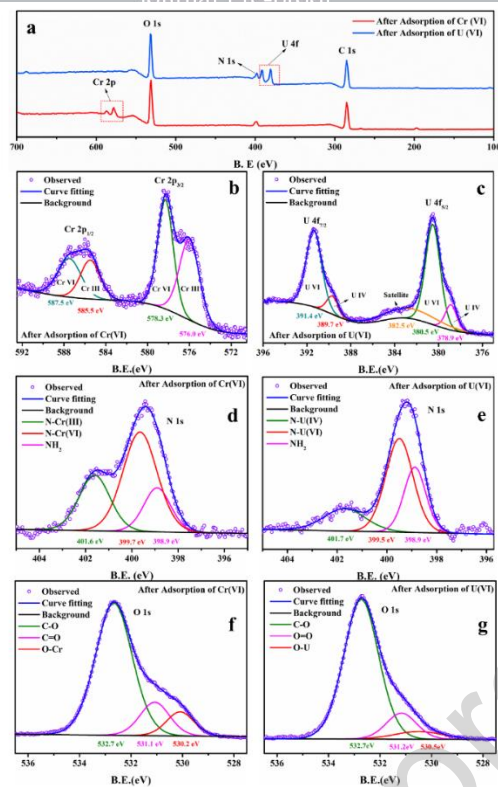


Figure 7. The XPS spectra of CS-TFT after the adsorption of Cr(VI) and U(VI): (a) full scan, and high-resolution spectrum of (b) Cr2p, (c) U4f, (d, e) N1s, and (f, g) O1s

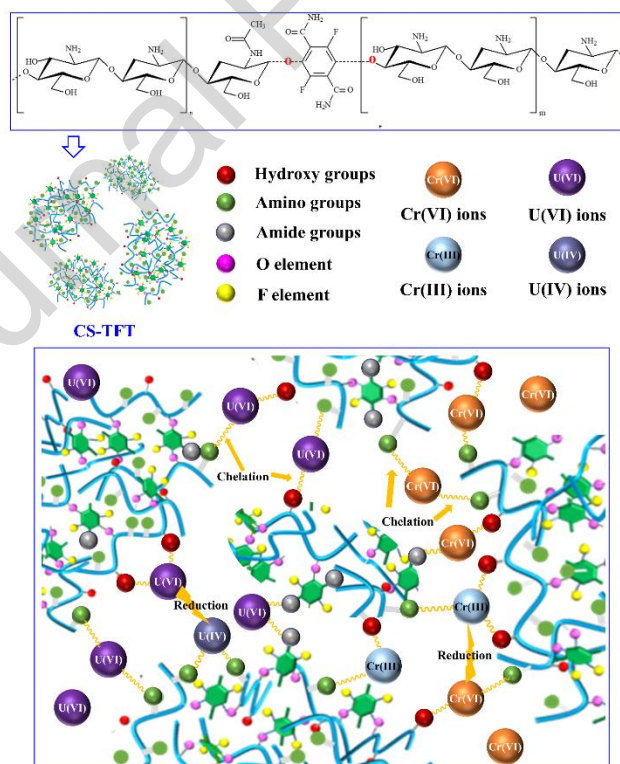


Figure 8. The scheme of the adsorption mechanism of Cr(VI) and U(VI) on CS-TFT.

Declaration of interests

The authors declare that they have no known competing financial interests or personal relationships that could have appeared to influence the work reported in this paper.

The authors declare the following financial interests/personal relationships which may be considered as potential competing interests:

Journal Pre-proof

Highlights

- CS-TFT is an innovative adsorbent prepared by cross-linking reaction.
- Efficient removal of Cr(VI) and U(VI) by CS-TFT even after 6 cycles.
- The adsorption kinetics follow a pseudo-second-order model.
- Chemisorption of Cr(VI) and U(VI) on CS-TFT.
- The adsorption mechanism has been proposed.

Journal Pre-proof